crystals

MDPI

Article

TiO_2-SnS_2 Nanoheterostructures for High-Performance Humidity Sensor

Wencheng Yu [1], Duo Chen [1,2,*], Jianfei Li [1,*] and Zhenzhen Zhang [1,2,*]

[1] International School for Optoelectronic Engineering, Qilu University of Technology (Shandong Academy of Science), Jinan 250353, China
[2] Laser Institute, Shandong Academy of Sciences, Jinan 250100, China
* Correspondence: drdchen@qlu.edu.cn (D.C.); jfl@qlu.edu.cn (J.L.); zzz@sdlaser.cn (Z.Z.)

Abstract: The larger surface-to-volume ratio of the hierarchical nanostructure means it has attracted considerable interest as a prototype gas sensor. Both TiO_2 and SnS_2 can be used as sensitive materials for humidity sensing with excellent performance. However, TiO_2-SnS_2 nanocomposites are rarely used in humidity detection. Therefore, in this work, a new humidity sensor was prepared by a simple one-step synthesis process based on nano-heterostructures, and the humidity sensing performance of the device was systematically characterized by much faster response/recovery behavior, better linearity and greater sensitivity compared to pure TiO_2 or SnS_2 nanofibers. The enhanced sensitivity of the nanoheterostructure should be attributed to its special hierarchical structure and TiO_2-SnS_2 heterojunction, which ultimately leads to a significant change in resistance upon water molecule exposure. In consideration of its non-complicated, cost-effective fabrication process and environmental friendliness, the TiO_2-SnS_2 nanoheterostructure is a hopeful candidate for humidity sensor applications.

Keywords: humid sensor; TiO_2-SnS_2 nanoheterostructure; composite

Citation: Yu, W.; Chen, D.; Li, J.; Zhang, Z. TiO_2-SnS_2 Nanoheterostructures for High-Performance Humidity Sensor. *Crystals* **2023**, *13*, 482. https://doi.org/10.3390/cryst13030482

Academic Editor: Arcady Zhukov

Received: 19 February 2023
Revised: 4 March 2023
Accepted: 7 March 2023
Published: 11 March 2023

1. Introduction

In recent years, semiconductor composites have become one of the hottest topics all over the world. When two different semiconductors are combined together, some novel properties may appear. TiO_2-MoS_2 [1] and TiO_2-Sn_3O_4 [2] show an enhanced photocatalytic activity. TeO_2-SnO_2 [3] and CuO-ZnO [4] have improved gas-sensing properties. Similarly, TiO_2-SnO_2 [5] and TiO_2-ZnO [6] display excellent ultraviolet responsivity. Metal oxides are stable in structure; easy to synthesize; have good application prospects in photoelectric measurement, gas detection, etc.; and are a class of cost-effective materials. Among metal oxide semiconductors, titanium dioxide (TiO_2) is one of the most widely used wide-band-gap oxide semiconductors. It has excellent physical and chemical properties and low prices and has been widely used in practical life. Since Fujisima and Honda published their work on the catalytic water splitting of TiO_2 under ultraviolet light irradiation in the 1970s [7], the application of TiO_2 has been rapidly extended to the fields of optoelectronics [8], photocatalysis [9], photo/electrochromic [10] and gas detection [11]. Moreover, TiO_2 has good chemical stability and controllable morphology and is a good matrix material [12]. As an n-type semiconductor material, SnS_2 belongs to layered metal sulfide with a hexagonal CdI_2 crystal structure, and it is a novel two-dimensional material [13]. SnS_2 has a wide energy band gap (about 2.18 eV [13]) and strong anisotropic optical properties. Therefore, SnS_2 is often used in gas-sensitive materials [14], photoelectric equipment [15], optical materials [16] and other fields. TiO_2 and SnS_2 have been studied as active materials in humidity sensors. A humidity sensor based on sol–gel-prepared TiO_2 film has been reported by Giampiero Montesperelli et al., which shows high humidity sensitivity at the minimum relative humidity (RH) values (4–10% RH) at 40 °C [17]. Lakshmi Deepika Bharatula et al. demonstrated a SnS_2 nanoflake micro-nano sensor device that can work within the scope of

11–97% RH at room temperature [18]. TiO_2-SnS_2 nanocomposites are generally used as photocatalytic materials. For example, Marin Kovacic et al. used TiO_2-SnS_2 nanocomposites as solar-active photocatalytic materials for water treatment [19]. Then, in the field of humidity sensors, carbon-based nanomaterials are commonly used as sensing materials. Due to the large specific surface area of carbon nanotubes, they have good adsorption characteristics for water molecules and are good moisture-sensitive materials for humidity sensors, and they also meet the development trend of the integration and miniaturization of humidity sensors. Hai M. Duong et al. used a high-temperature CVD furnace to produce continuous macroscopic fibers and films made from CNT superfibers and used them in the field of humidity sensing [20]. In addition, Hai Minh Duong et al. found that since the properties of post-treated CNT fibers are comparable to many commercial high-strength fibers, such as carbon fiber T300, Dyneema and Twaron, they can be utilized as reinforcements for advanced composites. Nanotube-based composites made from unstructured CNT powder have been extensively applied as structural materials for a wide range of applications, such as automotive and aerospace applications [21]. Therefore, carbon-based nanomaterials also have a wide range of promising applications.

In the investigations to date, many TiO_2 and SnS_2-related composites have been used in humidity sensors. Dongzhi Zhang et al. fabricated a humidity sensor based on a WS_2/SnO_2 nanocomposite with improved sensitivity and rapid response compared to pure WS_2 and pure SnO_2, and it also performs quite well in detecting human respiration [22]. Dongzhi Zhang et al. prepared SnS_2/Zn_2SnO_4 hybrid spherical films as sensitive materials for humidity sensors utilizing a layer-by-layer self-assembly technique. They found that the SnS_2/Zn_2SnO_4 hybrid thin-film sensors made significant progress in humidity sensors compared to single-SnS_2 and single-Zn_2SnO_4 nanomaterials, achieving accurate measurements of human breath, sweat, urine and water droplets [23]. Yun Wang et al. successfully fabricated tubular TiO_2-SnO_2 fibers (FIT-TSF) using a general crystal-phase-induced formation strategy. The prepared FIT-TSF exhibited excellent sensing performance with third-order impedance variation, an ultra-fast response time of 5 s, a recovery time of 8 s and good reproducibility [24]. Irene Cappelli et al. analyzed the performance of different humidity sensors based on TiO_2 nanoparticles and correlated them with different chemical/physical phenomena, and they found that when relative humidity is greater than 70%, the presence of condensate changes the electrical properties of the sensor, resulting in a smaller equivalent resistance value and a larger equivalent capacitance value of the sensor. The sensor has the advantages of a relatively fast response, a large measurement range and good stability [25]. However, there are few studies using TiO_2-SnS_2 nanocomposites for humidity detection.

In this paper, we synthesized high-quality TiO_2 nanoribbons by the hydrothermal method and acid treatment, and we dispersed SnS_2 nanoparticles on TiO_2 nanoribbons to form TiO_2-SnS_2 nanoheterostructures. The morphology and structure of bare TiO_2 nanoribbons and SnS_2-TiO_2 nanoheterostructures were characterized by transmission electron microscopy, scanning electron microscopy, Raman spectrum and X-ray diffraction. The optical properties of the bare TiO_2 and TiO_2-SnS_2 nanoheterostructures were characterized by reflection spectroscopy. The humidity sensors were prepared using bare TiO_2 nanoribbons, SnS_2 nanoparticles and TiO_2-SnS_2 nanoheterostructures as active materials, and their humidity detection performance at room temperature was investigated. Finally, through comparative experiments, we found that the resistance changes of the detector based on TiO_2-SnS_2 are linear with the relative humidity, while the resistance change of the two detectors based on pure TiO_2 and pure SnS_2 is not linear in the process of humidity change. In addition, the resistance of the two detectors based on pure TiO_2 and pure SnS_2 can reach 10^{10} ohms under low relative humidity, which is difficult to measure accurately. The resistance of TiO_2-SnS_2 is only in the order of kiloohms, which can be easily detected with an ordinary multimeter. This is coupled with the fact that the synthesis process of TiO_2-SnS_2 nanoheterostructures in this work is simpler and less costly than that of general metal

oxide composites. Therefore, the humidity sensor based on a TiO_2-SnS_2 nanostructure is more suitable for daily applications.

2. Materials and Methods

Analytically pure Titania P25 (TiO_2: ca. 80% anatase (CAS. 13463-67-7) and 20% rutile (CAS. 1317-80-2)), sodium hydroxide (NaOH (CAS. 1310-73-2)), hydrochloric acid (HCl (CAS. 7647-01-0)), sulfuric acid (H_2SO_4 (CAS. 7664-93-9)), tin(IV) chloride ($SnCl_4 \cdot 5H_2O$ (CAS. 10026-06-9)) and thioacetamide (CAS. 62-55-5) were used without further purification. A homogeneous solution was made by mixing 0.8 g of P25 TiO_2 with 80 mL of aqueous 10 M NaOH. The mixture was then shifted to a 100 mL Teflon (CAS. 9002-84-0) stainless steel autoclave and heated at 180 °C for 72 h. $Na_2Ti_3O_7$ nanoparticles were gained after thoroughly washing the obtained powder with deionized water. $H_2Ti_3O_7$ nanospheres were produced by immersing 0.47 g of $Na_2Ti_3O_7$ nanospheres into 58.8 mL of 0.1 M hydrochloric acid for 24 h. Finally, $H_2Ti_3O_7$ nanospheres (0.285 g) were etched in 14.25 mL of 0.02 M H_2SO_4 aqueous solution at 100 °C for 2 h to obtain rough nanospheres. The products were separated from the solution by centrifugation, washed thoroughly with deionized water in turn, and then annealed at 600 °C for 2 h to obtain TiO_2 nanospheres.

TiO_2-SnS_2 nanoheterostructures were prepared by a simple hydrothermal co-precipitation method. In a typical process, 2.5 mmol $SnCl_4 \cdot 5H_2O$ and 25 mmol thioacetamide were dissolved in 18 mL of deionized water to make a transparent solution, to which a certain amount of pre-synthesized TiO_2 nanobelts (molar ratio of Sn/Ti = 1/1) was added. Then, the solution was injected into a 20 mL Teflon-lined stainless-steel autoclave and maintained at 160 °C for 12 h. The obtained TiO_2-SnS_2 nanoheterostructures were washed with deionized water and dried at 70 °C. Bare SnS_2 was also prepared using a similar method.

The synthesized powders were dispersed in deionized water. Then, several drops of the obtained suspension were directly dropped onto a precleaned alumina (CAS. 1344-28-1) substrate, followed by thermal annealing at 100 °C for 30 min. Finally, interlaced gold electrodes (width: 100 μm; pitch: 200 μm) were deposited on the sample surface by thermal evaporation for humidity detection measurements.

The crystal structure of the samples was examined by X-ray diffraction (XRD, XD-3, PG Instruments Ltd., Beijing, China) and Raman (Bruker, Ltd., Billerica, MA, USA). The surface morphology of the samples was characterized by using field emission scanning electron microscopy (SEM; Hitachi S-4800, Hitachi, Ltd., Chiyoda, Tokyo, Japan). Transmission electron microscopy (TEM) and scanning transmission electron microscopy (STEM) were collected on a JEOL JEM 2100F electron microscope (JEM 2100F, JEOL Ltd., Tokyo, Japan) with an accelerating voltage of 200 kV. We used a saturated salt solution humidity generator to measure the humidity sensitivity of the sample. LiCl- (CAS. 7447-41-8), $MgCl_2 \cdot 6H_2O$- (CAS. 7791-18-6), NaBr- (CAS. 7647-15-6), NaCl- (CAS. 20510-56-9), KCl- (CAS. 7447-40-7) and KNO_3- (CAS. 14797-55-8) saturated salt solutions, whose corresponding humidity at room temperature was 11.30%, 32.78%, 57.57%, 75.29%, 84.34% and 93.58%, respectively, were chosen as humidity generators. Taking the relative humidity of the lithium-chloride-saturated salt solution as the background humidity, the response of TiO_2, SnS_2 and TiO_2-SnS_2 was measured under different moderate conditions.

3. Results and Discussion

As illustrated in Figure 1, the crystal structure of the synthetic TiO_2 nanobelts and TiO_2-SnS_2 nanoheterostructures was investigated by XRD. Figure 1a depicts the XRD pattern of TiO_2 nanobelts, with all diffraction peaks matching those of anatase TiO_2 (JCPDS card, no. 21-1272). For the TiO_2-SnS_2 (Figure 1b), besides the diffraction peaks from anatase TiO_2, all other peaks can be indexed to hexagonal-structured SnS_2 (JCPDS card, no. 23-0677). Figure 2 shows the Raman spectrums of TiO_2, SnS_2 and TiO_2-SnS_2. For the TiO_2, as shown in Figure 2a, three distinct peaks, centered at 237, 252 and 294 cm^{-1}, can be observed. Figure 2b shows the Raman spectral lines of the SnS_2 that has one distinct peak, centered at 310 cm^{-1}. The red curve in Figure 2 shows that the TiO_2-SnS_2 has three peaks centered at

235, 257 and 285 cm^{-1}, which roughly correspond to the three distinct peaks of TiO_2, and has one peak centered at 309 cm^{-1}, corresponding to the peak of SnS_2. No unambiguous signal from others is observed. These results confirm the successful deposition of SnS_2 on TiO_2 nanobelts, which is further proved by SEM and TEM in the following part.

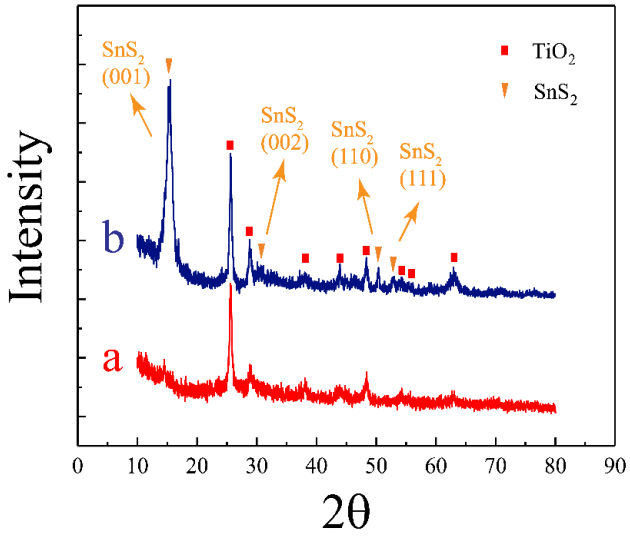

Figure 1. XRD patterns of (**a**) the TiO_2 belts and (**b**) the TiO_2-SnS_2 nanostructure.

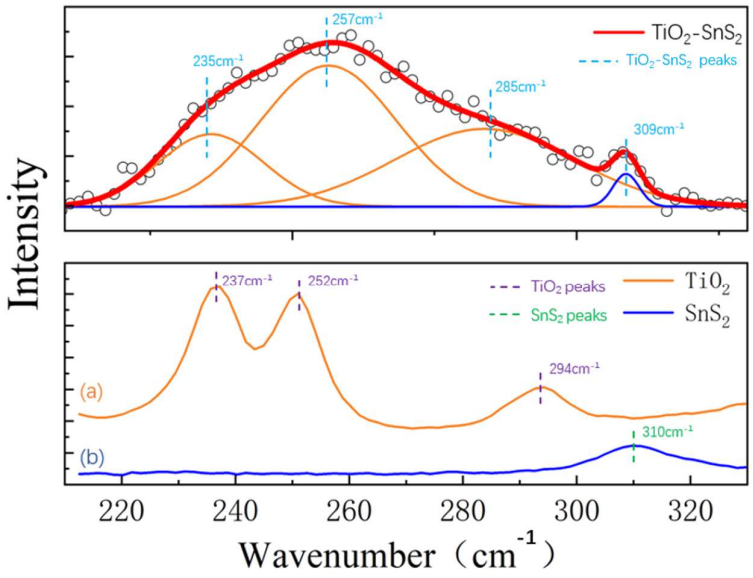

Figure 2. Raman spectrums of (**a**) the TiO_2, (**b**) the SnS_2 and the TiO_2-SnS_2.

Figure 3 shows the SEM images of the TiO_2 nanobelts and the TiO_2-SnS_2 nanoheterostructures. The surface of the TiO_2 nanobelts is relatively smooth, and the nanobelts are straight, as shown in Figure 3a. A higher-magnification SEM image (Figure 3b) shows that there are many randomly distributed dark depressions on the nanobelts as a result of the acid etching of the nanobelts. The morphology of the TiO_2-SnS_2 is shown in Figure 3c. The surface of the TiO_2 nanobelts is rough due to the deposition of SnS_2 nanoparticles. For better observation, a single-TiO_2 nanobelt decorated with SnS_2 is checked under high magnification, as shown in Figure 3d. It can be observed that the SnS_2 nanoparticles are scattered on the TiO_2 nanoribbons in a random shape.

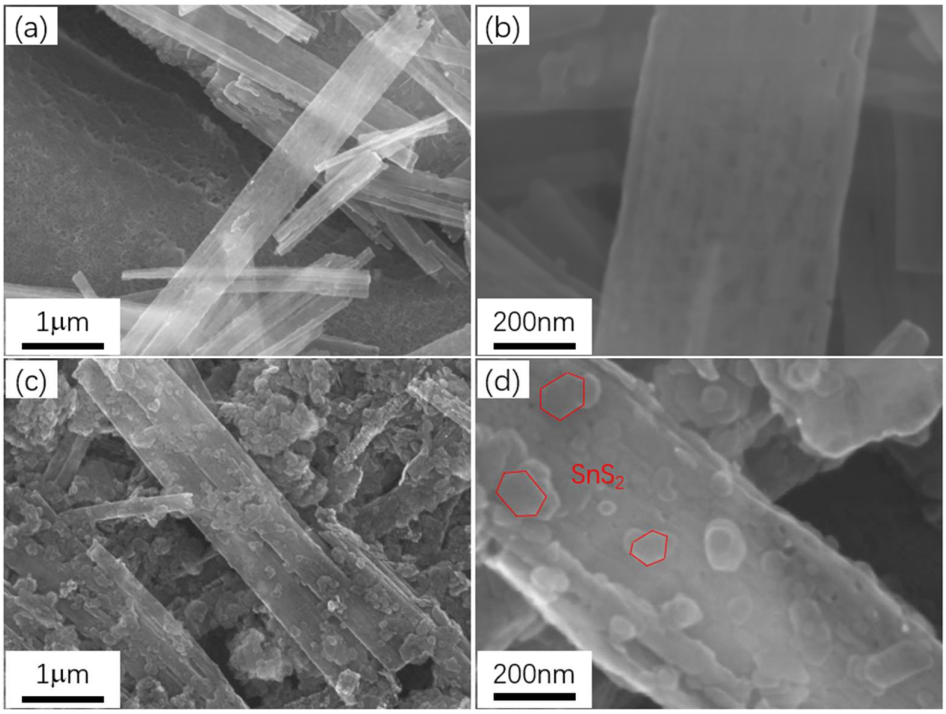

Figure 3. SEM images of (**a**,**b**) the TiO_2 nanobelts and (**c**,**d**) the TiO_2-SnS_2.

The morphology of the TiO_2 nanobelts is characterized by TEM, as shown in Figure 4a. The nanobelts are uniform and straight, with widths of 60–180 nm. A higher-magnification TEM image (Figure 4b) shows that there are many bright and dark regions randomly distributed on the nanobelts, which indicates that the nanobelt surface becomes rough due to acid etching. However, the single-crystal structure of TiO_2 is reserved even after acid etching, as demonstrated by HRTEM and the electron diffraction pattern in Figure 4c. The morphology of the TiO_2-SnS_2 nanostructure is shown in Figure 4d. SnS_2 nanoparticles are deposited on the surface of the TiO_2 nanobelt evenly. In order to facilitate better observation, a SnS_2-decorated single-TiO_2 nanobelt is checked at high magnification, as shown in Figure 4e. It can be seen that the size of SnS_2 nanoparticles is small and relatively homogeneous. As exhibited by HRTEM analysis of the TiO_2-SnS_2 nanoheterostructure in Figure 4f, SnS_2 nanoparticles with a size of approximately 10 nm are distributed on the TiO_2 nanobelt uniformly and densely.

Figure 5a shows the optical reflection spectra of bare TiO_2 and TiO_2-SnS_2 nanoheterostructures. A sharp decrease in the reflectivity can be observed at approximately 560 nm for TiO_2-SnS_2 and 370 nm for TiO_2, which can be attributed to the interband absorption of TiO_2-SnS_2 [26,27] and anatase TiO_2 [28]. The TiO_2-SnS_2 nanostrcuture exhibits lower reflection than the bare TiO_2 in visible light, which comes from the increased light absorption by SnS_2 nanoparticles [29]. Figure 5b shows the plots of $(F(R)E)^2$ as a function of photon energy E for TiO_2-SnS_2 and TiO_2 samples (F(R) is the Kubelka–Munk function; $F(R) = (1-R)^2/2R$, where R is the reflectance). The band gap can be determined by the linear extrapolation of $(F(R)E)^2$ to 0. The deduced band gap is about 3.36 eV for TiO_2 and 2.31 eV for TiO_2-SnS_2. Because of its strong absorption in visible light, the TiO_2-SnS_2 nanostructure may be used as the active layer in a visible-light photodetector.

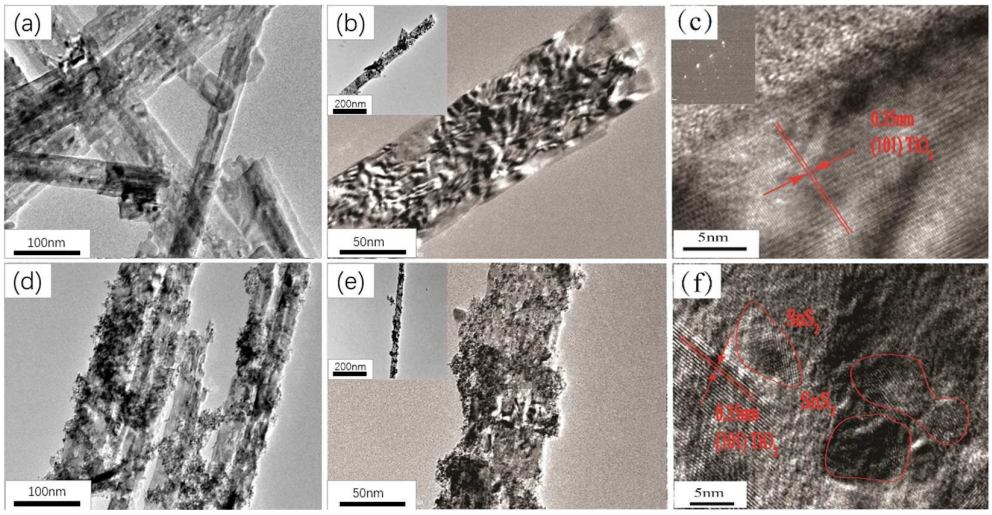

Figure 4. TEM images (**a**,**b**) and HRTEM image (**c**) of the TiO_2 nanobelts. TEM images (**d**,**e**) and HRTEM image (**f**) of TiO_2-SnS_2. Insets: (b) TEM image of single-TiO_2 nanobelt, (**c**) the electron diffraction pattern image of TiO_2 and (**e**) TEM image of single-SnS_2-TiO_2 nanoheterostructure.

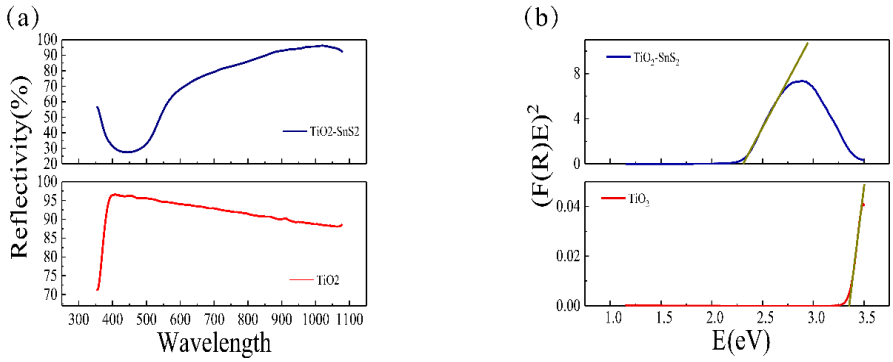

Figure 5. (**a**) The reflection spectra of TiO_2-SnS_2 and TiO_2 nanobelts. (**b**) Plots of $(F(R)E)^2$ versus photon energy E.

A saturated salt solution humidity generator, also known as a fixed-point humidity generator, has lots of advantages, such as simple equipment, cost-effectiveness, stable humidity value, easy recovery after damage, good reproducibility and so on. In this article, the humidity sensitivity of samples is measured using the saturated salt solution humidity generator. LiCl-, $MgCl_2 \cdot 6H_2O$-, NaBr-, NaCl-, KCl- and KNO_3-saturated salt solutions, whose corresponding humidity at room temperature is 11.30%, 32.78%, 57.57%, 75.29%, 84.34% and 93.58%, respectively, are chosen as humidity generators. The relative humidity of LiCl-saturated salt solution is taken as the background humidity, and the response curves of TiO_2, SnS_2 and TiO_2-SnS_2 at different humidity levels are shown in Figure 6. As shown in Figure 6a, the resistance of the SnS_2-TiO_2-based sensor is much smaller than that of the bare TiO_2 or SnS_2-based sensor, and the change in resistance from RH 11% to RH 93% reaches three orders of magnitude. However, in low relative humidity, the TiO_2 nanobelt device is in a high-resistance state (Figure 6b), and the resistance value is too high for an ordinary instrument. The response at different RH of the SnS_2 device is shown in Figure 6c. The resistance of this device is basically unchanged at lower RH, and the resistance change reaches three orders of magnitude from low RH to high RH. Figure 6d–f show the resistance of TiO_2-SnS_2, TiO_2 and SnS_2 sensors at different RH from 32.78% to 93.58%. The resistance change of the TiO_2-SnS_2 device is close to a linear relation, while the performance of the other two devices is unsatisfactory. Furthermore, the resistance of TiO_2 or SnS_2 devices reaches 10^{10} ohm, which is hard to be detected by ordinary instruments. In comparison,

the resistance of TiO_2-SnS_2 is only in the order of kiloohm, which can be easily detected by a multimeter. In other words, the device based on TiO_2-SnS_2 nanostructures is more practical for daily-life applications.

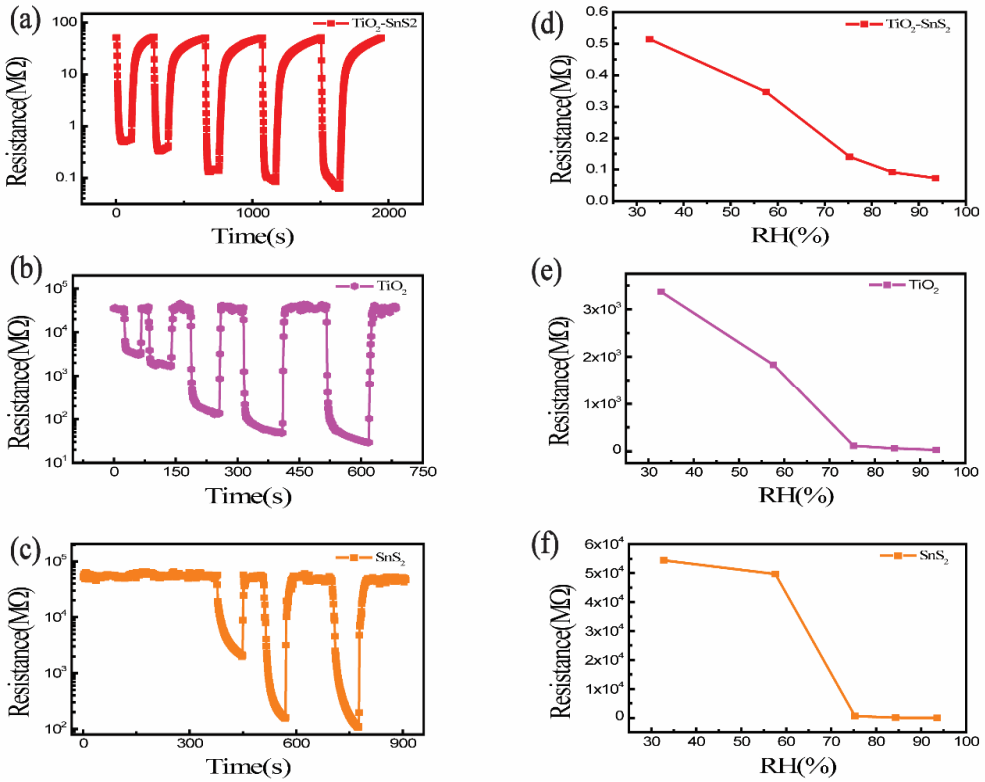

Figure 6. The humid responsivity (**a**) and (**d**) at different RH of TiO_2-SnS_2, the humid responsivity (**b**) and (**e**) at different RH of TiO_2, and the humid responsivity (**c**) and (**f**) at different RH of SnS_2.

Pure TiO_2 and SnS_2 have different responses to humidity, and the composite of the two materials TiO_2-SnS_2 shows different response mechanisms. First of all, we describe the sensing mechanisms of monolithic components (i.e., pure TiO_2 and SnS_2). The moisture sensing of TiO_2 is mainly caused by oxygen vacancies [30], and compounds containing alkali ions usually show significant hydrophilic properties due to their surface alkalinity [31]. When H_2O combines with variations, the conductivity is promoted. For SnS_2, the sensing mechanism here is dominant by proton conduction [32]. If abundant water molecules were adsorbed at the SnS_2 surface, proton conduction would be formed. As Figure 7a shows, when SnS_2 (band gap E_g = 2.18 eV [13]) loads on TiO_2 (E_g = 3.2 eV [33]), a potential barrier develops at the TiO_2-SnS_2 heterojunction. The equivalent resistance of the whole system is the series resistance of the R_t, R_s and R_h. R_t means the resistance of TiO_2, R_s means the resistance of SnS_2, and R_h means the resistance of the heterojunction. When the sensor is exposed to a low relative humidity environment, water molecules are adsorbed on the TiO_2 surface. It reduces the R_t. Therefore, equivalent resistance reduces. As the relative humidity increases, water molecules are further adsorbed due to the electrostatic effect of the OH- groups, and a physical adsorption water layer is formed [34]. Protons transfer from water molecules to SnS_2, and the potential barrier height reduces further, as shown in Figure 7b. The layer facilitates the transfer of H_2O or H_3O^+ [35,36]. The quick transfer of ions in the aqueous layer significantly decreases the impedance, which gives rise to the high sensitivity of the sensor.

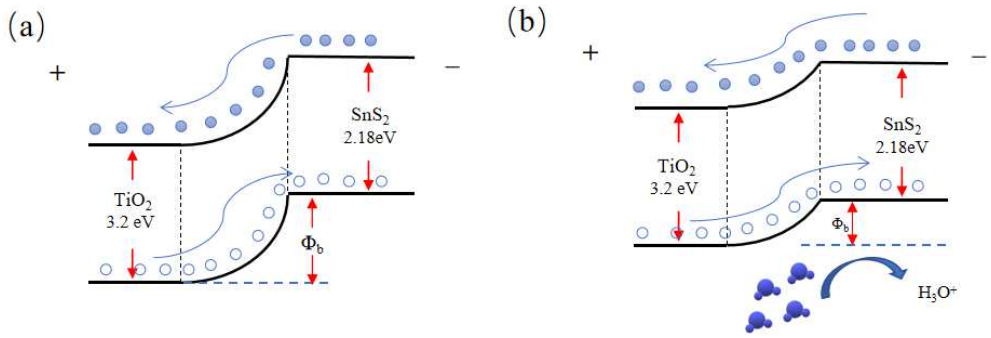

Figure 7. The energy band variations of the TiO_2-SnS_2 heterojunction after adsorbing water molecules at (**a**) without water and (**b**) with water.

Table 1 shows a comparison of the performance of some humidity sensors using various materials as sensitive materials. The main comparisons are made in terms of the fabrication method, measuring range, and response time. From the aspect of the fabrication method, this work uses a one-step hydrothermal method to prepare the samples, and the production process is relatively simple. From the aspect of measuring range, other parts of the material are similar to the samples prepared in this work and all have a large measurement range. From the aspect of response time, there exist other sensitive materials with more rapid response times, but the response time of the samples in this work is also faster. Dongzhi Zhang et al. used a simple one-step hydrothermal route for the preparation of microelectrode polyimide substrates to synthesize SnO_2 nanoparticles and SnO_2/RGO hybrids using hydrothermal methods and used them as sensitive materials to fabricate humidity sensors [37]. The sensor has the advantages of high sensitivity and fast measurement speed, but processing the material into a sensor is relatively tedious. Ravindra Kumar Jha and Prasanta Kumar Guha synthesized WS_2 nanosheets in a binary mixture of acetone and acetone by ultrasound and used them as a sensing material for a humidity sensor [38]. The sensor has a good linear relationship with the response of humidity, and the repeatability and stability are also good, but the disadvantage of this sensor is that the measurement range is relatively small. Ming-Zhi Yang et al. fabricated an integrated humidity microsensor using a commercial 0.18 μm complementary metal oxide semiconductor (CMOS) process [39]. The advantage of this sensing is the synthesis of a miniature humidity sensor that is very convenient, but one of the biggest limitations of this sensor is that the measurement range is too small. Yinghua Tan et al. prepared hollow MoS_2 micro@nano-sphere composites by a one-step hydrothermal method and used this material as a sensitive material to prepare humidity sensors [40]. They found that the sensor has high sensitivity and good stability through implementation, but the sensor has a relatively small measurement range compared to our humidity sensor. Hui Yang et al. prepared capacitive humidity sensors by sequentially coating aqueous suspensions of zinc oxide (ZnO) nanopowders and polyvinylpyrrolidone-reduced graphene oxide (PVP-RGO) nanocomposites dropwise on cross-finger electrodes [41]. The sensor showed a significant improvement in sensitivity and linearity compared with PVP RGO/ZnO, PVP-RGO and ZnO for the ZnO/PVP-RGO sensor. However, the preparation process of this sensor material is more tedious than the preparation process of the sensitive material used in this paper. Hengchang Bi et al. fabricated a miniature capacitive humidity sensor using a graphene oxide thin film as a humidity sensing material [42]. Compared with the conventional capacitive humidity sensor, this sensor has a high sensitivity at 15–95% relative humidity, which is more than 10 times more sensitive than the best of the conventional sensors. However, the fabrication process of this sensor is relatively tedious. Comparing all aspects, we can find that TiO_2-SnS_2 nanoheterostructures are indeed an excellent candidate to be used as sensitive materials for humidity sensors.

Table 1. Comparison of the main features of previously reported humidity sensors.

Active Materials	Fabrication Method	Measuring Range	Response	Reference
Graphene/SnO_2	Hydrothermal	11–97%RH	560.85	[37]
WS_2	Liquid exfoliation	40–80%RH	37.5	[38]
ZnO	Sol–gel method	40–90%RH	-	[39]
MoS_2	Hydrothermal	17.2–89.5%RH	67.34	[40]
ZnO/PVP/RGO	Drop-casting	15–95%RH	-	[41]
Graphene oxide	Solution dripping	15–95%RH	378	[42]
TiO_2-SnS_2	Hydrothermal	11–93%RH	60	This work

From the comparison of experimental results, the resistance of the TiO_2-SnS_2-based sensor is much smaller than that of the bare TiO_2 or SnS_2-based sensor, and the change in resistance from RH 11% to RH 93% reaches three orders of magnitude, from 0.05 MΩ to 100 MΩ. However, at low relative humidity, the TiO_2 nanoribbon devices are in a high resistance state, which is too high for ordinary instruments. The resistance of the SnS_2 nanoparticle devices is essentially unchanged at lower relative humidity, and the change in resistance from low to high relative humidity reaches three orders of magnitude. Resistance of the TiO_2-SnS_2 device varies linearly with humidity, while the other two devices do not perform as well. In addition, the resistance of TiO_2 or SnS_2 devices reaches 10^{10} ohms, which is difficult to detect with ordinary instruments. In contrast, the resistance of TiO_2-SnS_2 is only kiloohms, which can be easily detected with a multimeter. In addition, the roughness of the TiO_2 surface also affects the performance of the humidity sensor, which can be expressed as the larger the specific surface area of TiO_2, the better the effect of the humidity sensor, and conversely, the smaller the specific surface area of TiO_2, the worse the effect of the humidity sensor [43]. In terms of the humidity sensing performance of sensitive materials, the humidity sensors based on TiO_2-SnS_2 nanostructures are more suitable for everyday applications.

4. Conclusions

In summary, high-quality rough TiO_2 nanobelts were synthesized, and SnS_2 nanoparticles were loaded on the TiO_2 nanobelts by a hydrothermal method. The humidity detectors were fabricated using the powders of TiO_2-SnS_2, TiO_2 and SnS_2. Our research results show that the measurement range of TiO_2-SnS_2 nanoheterostructures in humidity detection is 11–93%, the response time is 60 s, and the linearity between resistance and humidity is good. In addition, the preparation of TiO_2-SnS_2 nanoheterostructures only uses a one-step hydrothermal method, the preparation process is very simple and convenient, and the cost of preparation is relatively low. These advantages will further increase the possibility of TiO_2-SnS_2 nanoheterostructures being excellent candidates for humidity detectors.

However, there are still some limitations to the TiO_2-SnS_2 we have synthesized. The structure of the TiO_2-SnS_2 nanoheterostructure we synthesized now is not very regular, and the performance of the humidity sensor needs to be further improved. In the next research, we will enhance the structure and number of heterojunctions, further modulate the structural properties of the interface to improve the humidity response of the sensor, and gradually explore the specificity of the sensor for some other gases to increase the practicality of the sensor.

Author Contributions: Conceptualization, D.C. and W.Y.; methodology, D.C.; software, W.Y.; validation, D.C.; formal analysis, W.Y.; investigation, J.L.; resources, D.C.; data curation, W.Y.; writing-original draft preparation, D.C.; writing-review and editing, W.Y.; visualization, J.L.; supervision, Z.Z.; project administration, Z.Z.; funding acquisition, D.C. All authors have read and agreed to the published version of the manuscript.

Funding: This work was supported by the Shandong Provincial Natural Science Foundation (ZR2021QF133), Basic research projects of science, education and industry integration pilot projects of Qilu University of Technology (2022PX037).

Data Availability Statement: The data that support the findings of this study are available within this article.

Acknowledgments: The authors acknowledge the experimental support of the International School for Optoelectronic Engineering at Qilu University of Technology (Shandong Academy of Science).

Conflicts of Interest: The authors declare no conflict of interest.

References

1. Jia, P.Y.; Guo, R.T.; Pan, W.G.; Huang, C.Y.; Tang, J.Y.; Liu, X.Y.; Qin, H.; Xu, Q.Y. The MoS_2/TiO_2 heterojunction composites with enhanced activity for CO_2 photocatalytic reduction under visible light irradiation. *Colloids Surf. A Physicochem. Eng. Asp.* **2019**, *570*, 306–316. [CrossRef]
2. Hu, J.; Tu, J.; Li, X.; Wang, Z.; Li, Y.; Li, Q.; Wang, F. Enhanced UV-Visible Light Photocatalytic Activity by Constructing Appropriate Heterostructures between Mesopore TiO_2 Nanospheres and Sn_3O_4 Nanoparticles. *Nanomaterials* **2017**, *7*, 336. [CrossRef] [PubMed]
3. Choi, M.S.; Bang, J.H.; Mirzaei, A.; Na, H.G.; Jin, C.; Oum, W.; Kim, S.S.; Kim, H.W. Exploration of the use of p-TeO_2-branch/n-SnO_2 core nanowires nanocomposites for gas sensing. *Appl. Surf. Sci.* **2019**, *484*, 1102–1110. [CrossRef]
4. Cai, L.; Li, H.; Zhang, H.; Fan, W.; Wang, J.; Wang, Y.; Wang, X.; Tang, Y.; Song, Y. High performance gas sensor based on ZnO/CuO heterostructures. In *Proceedings of 2019 International Conference on Optoelectronics and Measurement ICOM*; Springer: Singapore, 2021; Volume 726, pp. 191–198.
5. Chen, D.; Wei, L.; Meng, L.; Chen, Y.; Tian, Y.; Yan, S.; Mei, L.; Jiao, J. High-Performance Self-P formance Self-Powered UV Detected UV Detector Based or Based on SnO_2-TiO_2 Nanomace Arrays. *Nanoscale Res. Lett.* **2018**, *13*, 92. [CrossRef] [PubMed]
6. Shao, D.; Sun, H.; Xin, G.; Lian, J.; Sawyer, S. High quality ZnO–TiO_2 core–shell nanowires for efficient ultraviolet sensing. *Appl. Surf. Sci.* **2014**, *314*, 872–876. [CrossRef]
7. Fujishima, A.; Honda, K. Electrochemical photolysis of water at a semiconductor electrode. *Nature* **1972**, *238*, 37–38. [CrossRef] [PubMed]
8. Essalhi, Z.; Hartiti, B.; Lfakir, A.; Mari, B.; Thevenin, P. Optoelectronics properties of TiO_2: Cu thin films obtained by sol gel method. *Opt. Quantum Electron.* **2017**, *49*, 301. [CrossRef]
9. Nakata, K.; Fujishima, A. TiO_2 photocatalysis: Design and applications. *J. Photochem. Photobiol. C Photochem. Rev.* **2012**, *13*, 169–189. [CrossRef]
10. Şilik, E.; Pat, S.; Özen, S.; Mohammadigharehbagh, R.; Yudar, H.H.; Musaoğlu, C.; Korkmaz, Ş. Electrochromic properties of TiO_2 thin films grown by thermionic vacuum arc method. *Thin Solid Film.* **2017**, *640*, 27–32. [CrossRef]
11. Chen, D.; Yu, W.; Wei, L.; Ni, J.; Li, H.; Chen, Y.; Tian, Y.; Yan, S.; Mei, L.; Jiao, J. High sensitive room temperature NO_2 gas sensor based on the avalanche breakdown induced by Schottky junction in TiO_2-Sn_3O_4 nanoheterojunctions. *J. Alloys Compd.* **2022**, *912*, 165079. [CrossRef]
12. Hamidi, F.; Aslani, F. TiO_2-based Photocatalytic Cementitious Composites: Materials, Properties, Influential Parameters, and Assessment Techniques. *Nanomaterials* **2019**, *9*, 1444. [CrossRef]
13. Gaur, R.; Jeevanandam, P. Synthesis of SnS_2 Nanoparticles and Their Application as Photocatalysts for the Reduction of Cr(VI). *J. Nanosci. Nanotechnol.* **2018**, *18*, 165–177. [CrossRef] [PubMed]
14. Yang, Z.; Su, C.; Wang, S.; Han, Y.; Chen, X.; Xu, S.; Zhou, Z.; Hu, N.; Su, Y.; Zeng, M. Highly sensitive NO_2 gas sensors based on hexagonal SnS_2 nanoplates operating at room temperature. *Nanotechnology* **2019**, *31*, 075501. [CrossRef]
15. Han, X.; Xing, J.; Xu, H.; Huang, Y.; Li, D.; Lu, J.; Li, P.; Wu, Y. Remarkable improved photoelectric performance of SnS_2 field-effect transistor with Au plasmonic nanostructures. *Nanotechnology* **2020**, *31*, 215201.
16. Liu, M.; Wu, H.; Liu, X.; Wang, Y.; Lei, M.; Liu, W.; Guo, W.; Wei, Z. Optical properties and applications of SnS_2 SAs with different thickness. *Opto-Electron. Adv.* **2021**, *4*, 200029. [CrossRef]
17. Montesperelli, G.; Pumo, A.; Traversa, E.; Gusmano, E.; Bearzotti, A.; Montenero, A.; Gnappi, G. Sol—Gel processed TiO_2-based thin films as innovative humidity sensors. *Sens. Actuators B Chem.* **1995**, *25*, 705–709. [CrossRef]
18. Bharatula, L.D.; Erande, M.B.; Mulla, I.S.; Rout, C.S.; Late, D.J. SnS_2 nanoflakes for efficient humidity and alcohol sensing at room temperature. *RSC Adv.* **2016**, *6*, 105421–105427. [CrossRef]
19. Kovacic, M.; Kusic, H.; Fanetti, M.; Stangar, U.L.; Valant, M.; Dionysiou, D.D.; Bozic, A.L. TiO_2-SnS_2 nanocomposites: Solar-active photocatalytic materials for water treatment. *Environ. Sci. Pollut. Res.* **2017**, *24*, 19965–19979. [CrossRef] [PubMed]
20. Duong, H.M.; Tran, T.Q.; Kopp, R.; Myint, S.M.; Peng, L. Direct Spinning of Horizontally Aligned Carbon Nanotube Fibers and Films from the Floating Catalyst Method. In *Nanotube Superfiber Materials*, 2nd ed.; William Andrew Publishing: Norwich, NY, USA, 2019; pp. 3–29.
21. Duong, H.M.; Myint, S.M.; Tran, T.Q.; Le, D.K. Post-spinning treatments to carbon nanotube fibers. In *Carbon Nanotube Fibers and Yarns*; Elsevier: Amsterdam, The Netherlands, 2020; pp. 103–134.
22. Zhang, D.; Cao, Y.; Li, P.; Wu, J.; Zong, X. Humidity-sensing performance of layer-by-layer self-assembled tungsten disulfide/tin dioxide nanocomposite. *Sens. Actuators B Chem.* **2018**, *265*, 529–538. [CrossRef]
23. Zhang, D.; Zong, X.; Wu, Z.; Zhang, Y. Hierarchical Self-Assembled SnS_2 Nanoflower/Zn_2SnO_4 Hollow Sphere Nanohybrid for Humidity Sensing Applications. *ACS Appl. Mater. Interfaces* **2018**, *10*, 32631–32639. [CrossRef] [PubMed]

24. Wang, Y.; Zhao, X.; Feng, Z.; Lu, G.; Sun, T.; Xu, Y. Crystalline-phase-induced formation of fibre-in-tube TiO_2–SnO_2 fibres for a humidity sensor. *CrystEngComm* **2017**, *19*, 5528–5531. [CrossRef]
25. Cappelli, I.; Fort, A.; Lo Grasso, A.; Panzardi, E.; Mugnaini, M.; Vignoli, V. RH Sensing by Means of TiO_2 Nanoparticles: A Comparison among Different Sensing Techniques Based on Modeling and Chemical/Physical Interpretation. *Chemosensors* **2020**, *8*, 89. [CrossRef]
26. Shanmugaratnam, S.; Selvaratnam, B.; Baride, A.; Koodali, R.; Ravirajan, P.; Velauthapillai, D.; Shivatharsiny, Y. SnS_2/TiO_2 Nanocomposites for Hydrogen Production and Photodegradation under Extended Solar Irradiation. *Catalysts* **2021**, *11*, 589. [CrossRef]
27. Xia, F.F.; Yang, F.L.; Hu, J.; Zheng, C.Z.; Yi, H.B.; Sun, J.H. Enhanced visible light absorption performance of SnS_2 and $SnSe_2$ via surface charge transfer doping. *RSC Adv.* **2018**, *8*, 40464–40470. [CrossRef] [PubMed]
28. Nagaveni, K.; Hegde, M.S.; Ravishankar, N.; Subbanna, G.N.; Madras, G. Synthesis and Structure of Nanocrystalline TiO_2 with Lower Band Gap Showing High Photocatalytic Activity. *Langmuir* **2004**, *20*, 2900–2907. [CrossRef] [PubMed]
29. Gao, J.; Sun, X.; Zheng, L.; He, G.; Wang, Y.; Li, Y.; Liu, Y.; Deng, J.; Liu, M.; Hu, J. 2D Z-scheme TiO_2/SnS_2 Heterojunctions with Enhanced Visible-light Photocatalytic Performance for Refractory Contaminants and Mechanistic Insight. *New J. Chem.* **2021**, *45*, 16131–16142. [CrossRef]
30. Li, T.Y.; Si, R.J.; Sun, J.; Wang, S.T.; Wang, J.; Ahmed, R.; Zhu, G.B.; Wang, C.C. Giant and controllable humidity sensitivity achieved in (Na plus Nb) co-doped rutile TiO_2. *Sens. Actuators B Chem.* **2019**, *293*, 151–158. [CrossRef]
31. Boukoussa, B.; Hakiki, A.; Nunes-Beltrao, A.P.; Hamacha, R.; Azzouz, A. Assessment of the intrinsic interactions of nanocomposite polyaniline/SBA-15 with carbon dioxide: Correlation between the hydrophilic character and surface basicity. *J. CO2 Util.* **2018**, *26*, 171–178. [CrossRef]
32. HHassan, H.U.; Mun, J.; Kang, B.S.; Song, J.Y.; Kim, T.; Kang, S.-W. Sensor based on chemical vapour deposition-grown molybdenum disulphide for gas sensing application. *RSC Adv.* **2016**, *6*, 75839–75843. [CrossRef]
33. Zhang, H.; Gao, Y.; Zhu, G.; Li, B.; Gou, J.; Cheng, X. Synthesis of PbS/TiO2 nano-tubes photoelectrode and its enhanced visible light driven photocatalytic performance and mechanism for purification of 4-chlorobenzoic acid. *Sep. Purif. Technol.* **2019**, *227*, 115697. [CrossRef]
34. Anderson, J.H.; Parks, G.A. Electrical conductivity of silica gel in the presence of adsorbed water. *J. Phys. Chem.* **1968**, *72*, 3662–3668. [CrossRef]
35. Agmon, N. The Grotthuss mechanism. *Chem. Phys. Lett.* **1995**, *244*, 456–462. [CrossRef]
36. Casalbore-Miceli, G.; Yang, M.J.; Camaioni, N.; Mari, C.M.; Li, Y.; Sun, H.; Ling, M. Investigations on the ion transport mechanism in conducting polymer films. *Solid State Ion.* **2000**, *131*, 311–321. [CrossRef]
37. Zhang, D.; Chang, H.; Li, P.; Liu, R.; Xue, Q. Fabrication and characterization of an ultrasensitive humidity sensor based on metal oxide/graphene hybrid nanocomposite. *Sens. Actuators B Chem.* **2016**, *225*, 233–240. [CrossRef]
38. Jha, R.K.; Guha, P.K. Liquid exfoliated pristine WS_2 nanosheets for ultrasensitive and highly stable chemiresistive humidity sensors. *Nanotechnology* **2016**, *27*, 475503. [CrossRef]
39. Yang, M.Z.; Dai, C.L.; Wu, C.C. Sol-Gel Zinc Oxide Humidity Sensors Integrated with a Ring Oscillator Circuit On-a-Chip. *Sensors* **2014**, *14*, 20360–20371. [CrossRef]
40. Tan, Y.; Yu, K.; Yang, T.; Zhang, Q.; Cong, W.; Yin, H.; Zhang, Z.; Chen, Y.; Zhu, Z. The combinations of hollow MoS_2 micro@nano-spheres: One-step synthesis, excellent photocatalytic and humidity sensing properties. *J. Mater. Chem. C* **2014**, *2*, 5422–5430. [CrossRef]
41. Yang, H.; Ye, Q.; Zeng, R.; Zhang, J.; Yue, L.; Xu, M.; Qiu, Z.-J.; Wu, D. Stable and Fast-Response Capacitive Humidity Sensors Based on a ZnO Nanopowder/PVP-RGO Multilayer. *Sensors* **2017**, *17*, 2415. [CrossRef]
42. Bi, H.; Yin, K.; Xie, X.; Ji, J.; Wan, S.; Sun, L.; Terrones, M.; Dresselhaus, M.S. Ultrahigh humidity sensitivity of graphene oxide. *Sci. Rep.* **2013**, *3*, 2714. [CrossRef]
43. Zhao, X.; Chen, X.; Ding, X.; Yu, X.; Chen, X.; Liu, F. Humidity Sensing Properties and Negative Differential Resistance Effects of TiO_2 Nanowires. *IEEE Sens. J.* **2021**, *21*, 18477–18482. [CrossRef]